

Nonequilibrium dynamics in Dirac quantum criticality

Yin-Kai Yu,¹ Zhi Zeng,¹ Yu-Rong Shu,² Zi-Xiang Li,^{3,4,*} and Shuai Yin^{1,†}

¹*School of physics, Sun Yat-Sen University, Guangzhou 510275, China*

²*School of Physics and Materials Science, Guangzhou University, Guangzhou 510006, China*

³*Beijing National Laboratory for Condensed Matter Physics & Institute of Physics,
Chinese Academy of Sciences, Beijing 100190, China*

⁴*University of Chinese Academy of Sciences, Beijing 100049, China*

(Dated: October 17, 2023)

Quantum criticality within Dirac fermions harbors a plethora of exotic phenomena, attracting sustained attention in the past decades. Nevertheless, the nonequilibrium dynamics therein has rarely been studied. To fill in the gap, we explore the imaginary-time relaxation dynamics in a typical Dirac quantum criticality belonging to chiral Heisenberg universality class. Performing large-scale quantum Monte Carlo simulation, we unveil rich nonequilibrium critical phenomena from different initial states. Particularly, a new dynamic exponent characterizing the non-stationary evolution in the short-time state is determined as $\theta = -0.84(4)$, in sharp contrast with the prevalent belief that θ is positive as demonstrated in classical cases. Furthermore, we propose a universal dynamic scaling theory governing the fruitful nonequilibrium properties in Dirac quantum criticality. Armed with the scaling theory, we develop a new framework to investigate fermionic quantum criticality based on short-time dynamics, paving a promising avenue to fathoming quantum criticality in diverse fermionic systems with high efficiency.

Introduction— Quantum phase transitions, describing abrupt changes in ground states of quantum systems, remain central topics in modern physics [1]. A prominent example is the interaction-driven quantum criticality in Dirac systems. Such transitions were originally discussed in the high-energy physics to mimic chiral symmetry breaking and spontaneous mass generation [2]. Recently, owing to the inspiring experimental advances in graphene [3] and topological materials [4, 5], quantum criticality in Dirac fermions has garnered increasing interests in condensed matter physics. Vast efforts have been paid in this field, including sophisticated renormalization group analyses [6–17], conformal bootstrap [18], quantum Monte Carlo simulation [19–32] and tensor network method [33, 34], resulting in tremendous achievements. It was shown that fluctuations from gapless Dirac fermions enormously fertilize the fundamental research of quantum criticality, not only contributing to the Gross-Neveu fixed point [6–49], which is among the simplest examples of quantum critical points that do not exhibit classical analogs, but also yielding a profound mechanism for the Landau-forbidden quantum criticality [50–55].

On the other hand, equilibrium state in nature is just the exception rather than the norm. Universal critical phenomena are manifested not only in the long-time equilibrium states but also in short-time nonequilibrium processes [56–60]. For instance, in classical systems, after a sudden quench to the critical point, the relaxation dynamics shows a non-stationary initial slip evolution in the short-time stage [61–63]. Associated with this critical initial slip, it turns out that there exists an additional critical exponent that describes how the system remembers its initial information [61]. Similar short-time scaling behaviors are also found in the quench dynamics of quantum systems, wherein the universal dynamics

is shown to be controlled by a non-thermal fixed point, rather than the one describing the quantum phase transition in ground state [64–72].

Aside from the real-time dynamics, imaginary-time dynamics in quantum systems is also of great interest and significance. As a routine unbiased approach to identify the ground state, the imaginary-time evolution works not only extensively in numerical simulations, but also in vivifying quantum computers [73–75], which has been seeing fervent activity spurred by the recent availability of noisy intermediate-scale quantum hardware and provides a promising platform to explore various exotic quantum phases [76, 77]. Near a quantum critical point (QCP), it was shown that the imaginary-time critical dynamics demonstrates colorful universal scaling behaviors in both short-time and long-time stages [78–81]. So far, the imaginary-time relaxation dynamics has been studied in various quantum systems, providing an abundance of intriguing perspectives in the field of quantum criticality [81–85]. Moreover, the imaginary-time scaling has been observed in an experimental platform of quantum computer and shows its power in determining the critical properties with high efficiency and scalability in fast-developing quantum devices, circumventing difficulties induced by critical slowing down and divergent entanglement in conventional method based on equilibrium scaling [86].

However, the intriguing nonequilibrium dynamic behavior in Dirac quantum criticality has been sparsely explored to date. Given the unique universal physics inherent in Dirac systems, it is immensely desired to investigate the nonequilibrium properties in the presence of gapless Dirac fermions, and particularly, establish a general theoretical framework to describe the dynamic scaling behavior in Dirac quantum criticality. Here, we ex-

plore the imaginary-time critical dynamics of a paradigmatic Dirac-fermion quantum critical point, namely chiral Heisenberg Gross-Neveu quantum criticality hosted by the honeycomb Hubbard model [35–39]. Employing sign-problem-free QMC simulation [87–95], we unambiguously demonstrate that the system features rich short-time scaling behaviors for different initial states. We develop a general nonequilibrium scaling theory unifying these exotic scaling properties of short-time dynamics. In particular, with a disordered initial state, a novel critical initial slip behavior with a negative characteristic exponent is uncovered, which is remarkably different from the bosonic cases in which the critical initial slip exponent is usually positive. We point out that this anomalous behavior is attributed to the gapless fluctuations arising from Dirac fermions. Moreover, through the application of scaling theory of imaginary-time dynamics, we successfully determine the critical exponents of chiral Heisenberg Gross-Neveu quantum criticality, consistent with previous studies on equilibrium cases. Hence, our scaling theory offers not only a unified framework to understand nonequilibrium imaginary-time critical dynamics of Dirac systems, but also an amenable and innovative route to investigating the critical properties in strongly correlated systems.

Hamiltonian and quench protocol— To explore the dynamic scaling in chiral Heisenberg universality class, we start with the Hubbard model defined on the honeycomb lattice, characterized by the Hamiltonian [35–39]:

$$H = -t \sum_{\langle ij \rangle, \sigma} c_{i\sigma}^\dagger c_{j\sigma} + U \sum_i \left(n_{i\uparrow} - \frac{1}{2} \right) \left(n_{i\downarrow} - \frac{1}{2} \right), \quad (1)$$

in which $c_{i\sigma}^\dagger$ ($c_{j\sigma}$) represents the creation (annihilation) operator of electrons with spin polarization σ , $n_{i\sigma} \equiv c_{i\sigma}^\dagger c_{i\sigma}$ is the electron number operator, t is hopping amplitude between the nearest neighbor sites, and U represents the strength of on-site repulsive interaction. As shown in Fig. 1, when $U/t \ll 1$ the system is in the Dirac semimetal (DSM) phase characterized by the four-component Dirac excitation with flavor number $N_f = 2$; whereas for large $U/t \gg 1$ the system hosts an antiferromagnetic (AFM) phase with a finite charge gap. A phase transition separating these two phases happens at a finite $U_c/t \approx 3.9$ and belongs to the chiral Heisenberg universality class [35–39]. For simplicity, we set t to unity in subsequent discussions.

For the imaginary-time relaxation dynamics, the wave function $|\psi(\tau)\rangle$ evolves according to the imaginary-time Schrödinger equation

$$-\frac{\partial}{\partial \tau} |\psi(\tau)\rangle = H |\psi(\tau)\rangle, \quad (2)$$

imposed by the normalization condition. The formal solution of the Schrödinger equation is given by $|\psi(\tau)\rangle = e^{-\tau H} |\psi(0)\rangle / Z(\tau)$, in which $Z(\tau) \equiv \langle \psi(\tau) | \psi(\tau) \rangle$ is the

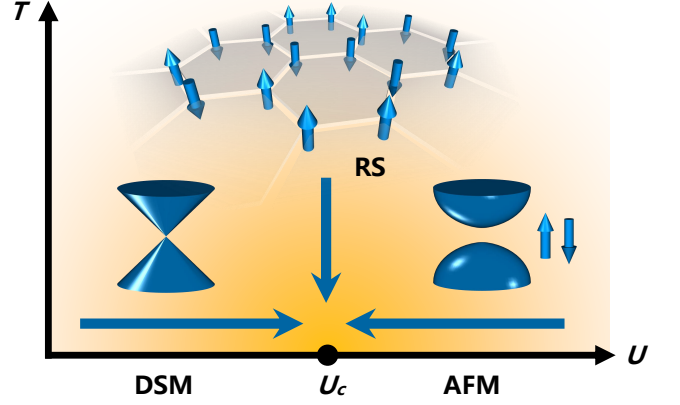


FIG. 1. Sketch of the phase diagram and the quench protocol in imaginary-time with different initial states. The initial states are prepared as (i) the Dirac semimetal (DSM) phase, (ii) the saturated AFM state, and (iii) the random spin (RS) state. All states correspond to the fixed points of the initial states under the renormalization group transformation.

normalization factor and $|\psi(0)\rangle$ is the initial wavefunction. As illustrated in Fig. 1, we will consider three kinds of initial states: (i) the saturated AFM state, (ii) the non-interacting DSM state, and (iii) the random spin (RS) state. In the following, we will employ the large-scale determinant quantum Monte Carlo (DQMC) method to investigate the imaginary-time relaxation dynamics. The model does not suffer from sign problem, such that it is feasible to access the numerically accurate properties with large system sizes.

General scaling theory— Near the critical point, the equilibration time tends to infinity in the thermodynamic limit, leading to a macroscopically long time scale of the remanent of the initial state. Generally, for an observable P its dynamic scaling should satisfy [81, 96]:

$$P(\tau, g, L, \{X\}) = \tau^{-\frac{\kappa}{z}} f_P \left(g \tau^{\frac{1}{\nu z}}, L^{-1} \tau^{\frac{1}{z}}, \{X \tau^{-\frac{c}{z}}\} \right), \quad (3)$$

in which $g \equiv (U - U_c)/t$, L is the lattice size. κ is the critical exponent related to the scaling dimension of P , and ν is the correlation length exponent. z is dynamical exponent, and $z = 1$ for the Dirac QCP in Eq. (1) because the nonrelativistic corrections are irrelevant. $\{X\}$ with its exponent c represents the possible relevant variables associated with the initial state.

Two remarks on Eq. (3) are listed as follows. (a) For $\tau \rightarrow \infty$, Eq. (3) recovers the usual finite-size scaling form and $\{X\}$ becomes irrelevant. (b) All three kinds of initial states studied here, namely AFM state, DSM state and RS state, correspond to three stable fixed points, respectively. Thus, $\{X\}$ does not explicitly appear in Eq. (3). However, the scaling functions f_P vary for different initial states.

Relaxation dynamics with AFM initial state— First, we study the relaxation dynamics starting with the

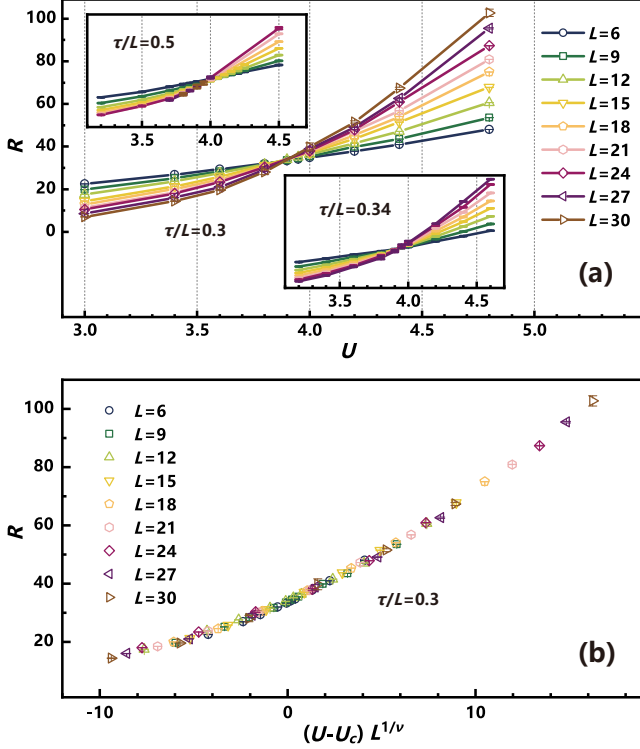


FIG. 2. The results of correlation-length ratio R against interaction U for various sizes during the short-time stage, with a fixed value of τL^{-z} . (a) Estimation of the critical point via the intersection points of curves for $\tau L^{-z} = 0.3$ (Main panel), 0.34 and 0.5 (Inset). (b) Estimation of ν by scaling collapse analysis of correlation-length ratio.

AFM initial state. To illustrate the nonequilibrium scaling properties, we explore the critical dynamics of the correlation-length ratio defined as [97]:

$$R \equiv S(\mathbf{0})/S(\Delta\mathbf{q}), \quad (4)$$

where $\Delta\mathbf{q}$ is minimum lattice momentum and $S(\mathbf{q})$ is the antiferromagnetic structure factor:

$$S(\mathbf{q}) = \frac{1}{L^{2d}} \sum_{i,j} e^{i\mathbf{q} \cdot (\mathbf{r}_i - \mathbf{r}_j)} \langle S_i^z S_j^z \rangle, \quad (5)$$

with S_i^z being the staggered magnetization operator defined as $S_i^z \equiv \vec{c}_{i,A}^\dagger \sigma^z \vec{c}_{i,A} - \vec{c}_{i,B}^\dagger \sigma^z \vec{c}_{i,B}$ and $\vec{c}^\dagger \equiv (c_\uparrow^\dagger, c_\downarrow^\dagger)$.

As a dimensionless variable, R in the relaxation process obeys the following dynamic scaling form according to Eq. (3):

$$R(g, \tau, L) = f_R(gL^{1/\nu}, \tau L^{-z}), \quad (6)$$

which indicates that with a fixed τL^{-z} the correlation-length ratio R does not depend on the system size when $g = 0$, thereby providing a method to pinpoint the critical point.

As shown in Fig. 2 (a), we calculate R as a function of U with fixed $\tau L^{-z} = 0.3$ for different sizes, and find

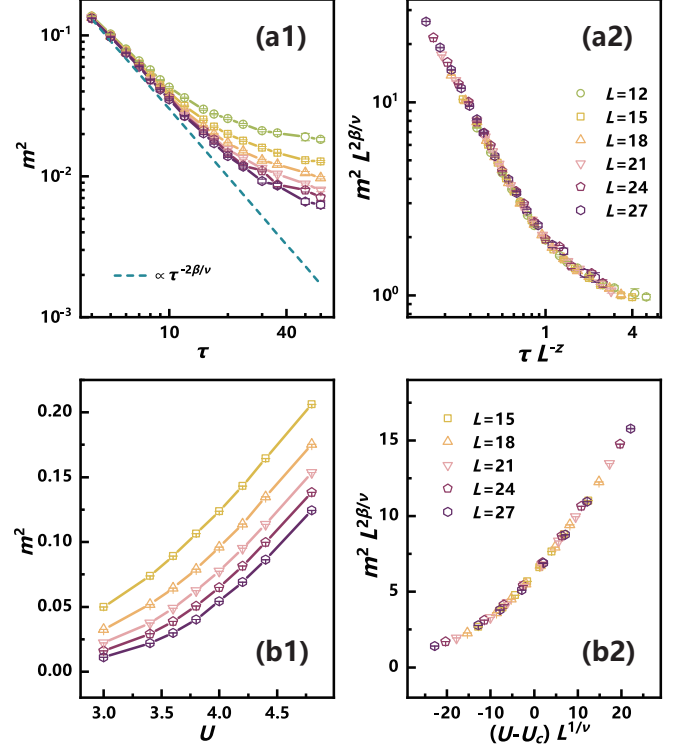


FIG. 3. Relaxation dynamics of the order parameter with the AFM initial state. (a) Curves of m^2 versus τ at the critical point for different sizes before (a1) and after (a2) rescaling. The dashed line representing $m^2 \propto \tau^{-2\beta/\nu}$ with β/ν estimated from (a2) is plotted in (a1) for comparison. (b) Curves of m^2 versus U with fixed $\tau L^{-z} = 0.3$ before (b1) and after (b2) rescaling.

that the curves almost cross at a point. By extrapolating the intersection points $U_c(L)$ between curves for $L+3$ and L to the thermodynamic limit according to $U_c(L) = U_c + aL^{-w}$, one can determine the critical point as $U_c = 3.91(3)$. Upon fixing $U_c = 3.91$ into Eq. (6), we adjust the value of ν for the rescaled horizontal variable $gL^{1/\nu}$ to make curves of different sizes collapse with each other, yielding the value of ν as $\nu = 1.17(7)$. Remarkably, both values of U_c and ν are consistent with those obtained from equilibrium finite-size scaling within one standard deviation, albeit slight deviations arise possibly due to the scaling corrections [8, 39]. However, significantly less effort is required as the results are obtained in the short-time stage and long enough imaginary-time evolution to achieve the ground state in the usual equilibrium method is not required here. Moreover, Eq. (6) also provides a self-consistent way to confirm the results. As shown in Fig. 2 and the supplementary materials [98], for different τL^{-z} , consistent U_c and ν are obtained in a similar way, highlighting the validity of Eq. (6).

To delve deeper into the relaxation dynamics governed by model (1), we study the dynamics of structure factor, namely the square of order parameter $m^2 = S(0)$. Ac-

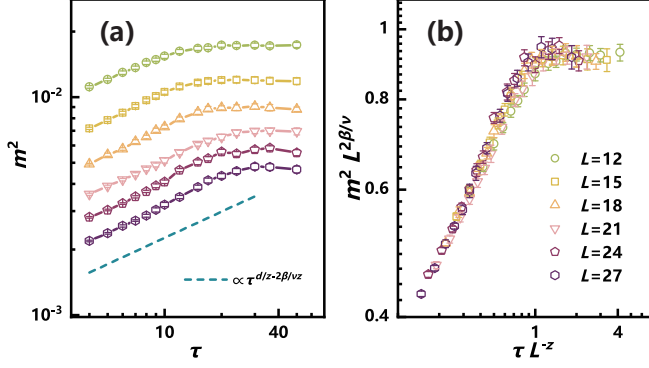


FIG. 4. Relaxation dynamics of the order parameter with the DSM initial state. Curves of m^2 versus τ at the critical point for different sizes before (a) and after (b) rescaling. The dashed line representing $m^2 \propto \tau^{d/(z-2\beta/\nu z)}$ is plotted in (a) for comparison. The critical exponents used here are estimated from Fig. 3 (a).

cording to Eq. (3), starting from a completely ordered AFM initial state, the decaying behavior of m^2 should satisfy [62, 81]:

$$m^2(g, \tau, L) = \tau^{-2\beta/\nu z} f_m(gL^{1/\nu}, \tau L^{-z}), \quad (7)$$

where β/ν is the exponent associated with scaling dimension of order parameter. Note that Eq. (7) is equivalent to $m^2(g, \tau, L) = L^{-2\beta/\nu} f_{m1}(gL^{1/\nu}, \tau L^{-z})$ so that the usual finite-size scaling is recovered as $\tau \rightarrow \infty$.

Figure 3 (a1) shows the evolution of m^2 at $g = 0$ for different system sizes. At first, as shown in Fig. 3 (a2), data collapse analysis of the results yields the exponent $\beta = 0.80(3)$, which is close to the result obtained in previous studies on equilibrium systems [38, 39]. The collapse of rescaled results for different systems sizes into a single curve unequivocally demonstrates the dynamic scaling behavior with AFM as initial state, as depicted in Eq. (7). Moreover, as shown in Fig. 3 (a1), one finds that in the short-time stage, $m^2 \propto \tau^{-2\beta/\nu z}$ and the scaling behavior is almost independent of the system size. The underlying reason is that the initial state is an uncorrelated state and the correlation length ξ increases with time as $\xi \propto \tau^{1/z}$. In the short-time stage, $\xi < L$ and the finite-size effects are negligible; whereas in the long-time stage, $\xi > L$ and the system enters the finite-size scaling region in which $m^2 \propto L^{-2\beta/\nu}$. These results demonstrate that it is feasible to infer the critical properties in the thermodynamic limit directly from the short-time dynamics.

Besides, for a fixed τL^{-z} , Eq. (7) reduces to $m^2(g, L) = L^{-2\beta/\nu} f_{m2}(gL^{1/\nu})$. Note that this scaling form is different from the equilibrium finite-size scaling since their scaling functions are different. Fig. 3 (b) depicts the dependence of m^2 on U for different system sizes at $\tau L^{-z} = 0.3$. By tuning the exponents to make the rescaled curves of m^2 versus g collapse, we determine the exponents as $\nu = 1.025(9)$ and $\beta/\nu = 0.735(2)$, as shown

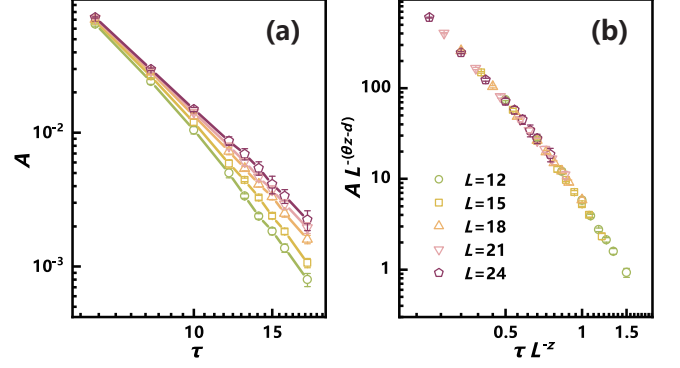


FIG. 5. Critical initial slip manifested in the evolution of the auto-correlation function A with the RS initial state. Curves of A versus τ for different sizes at the critical point before (a) and after (b) rescaling.

in Fig. 3 (b2). These values are also consistent with the previous results of equilibrium systems [39]. In this way, we further verify Eq. (7), and more crucially, determine the critical exponents from the nonequilibrium approach.

Relaxation dynamics with DSM initial state— We proceed to explore the relaxation dynamics from the non-interacting DSM state. For this state, it is straightforward to show that AFM structure factor obeys the scaling $m^2 \propto L^{-d}$. This size-dependent scaling affects the relaxation dynamics in the short-time stage, giving rise to the short-time dynamic scaling of m^2 :

$$m^2(g, \tau, L) = L^{-d} \tau^{d/(z-2\beta/\nu z)} f_{m3}(gL^{1/\nu}, \tau L^{-z}). \quad (8)$$

To demonstrate the dynamic scaling Eq. (8), we show in Fig. 4 the evolution of m^2 at the critical point, namely $g = 0$ in Eq. (8). In the short-time stage, m^2 increases as $m^2(g, \tau, L) \propto \tau^{d/(z-2\beta/\nu z)}$ for given L , qualitatively different from the dynamic behavior with AFM initial state; whereas in the long-time stage, m^2 begins to saturate. In addition, by rescaling m^2 and τ according to Eq. (3) with the exponents determined in previous section, one finds that the curves collapse onto each other. These results reveal the dynamic scaling behavior with DSM initial state described by Eq. (8).

Critical initial slip with RS initial state— Then we study the relaxation dynamics from the RS state, for which every site has one electron with its spin randomly distributed. Practically, this state can be prepared at a high temperature. With this uncorrelated initial state, the evolution of m^2 still satisfies Eq. (8) except for a different scaling function, as discussed in the supplementary materials [98].

Furthermore, when initiating from the RS state, we observe a universal critical initial slip behavior in the short-time stage. Intriguingly, the scaling property of the initial slip behavior is determined by an independent dynamic exponent θ , which does not exist in the equilibrium critical behavior. To characterize the critical initial

slip, the auto-correlation function A was introduced, defined as [61, 62]:

$$A = \frac{1}{L^d} \sum_i \overline{\langle S_i(0) \rangle \langle S_i(\tau) \rangle}, \quad (9)$$

where the overline denotes the average on the initial state configurations. At the critical point, the auto-correlation function obeys the following scaling form:

$$A(\tau) = \tau^{-d/z+\theta} f_A(\tau L^{-z}), \quad (10)$$

As shown in Fig. 5, by rescaling A and τ according to Eq. (10) and adjusting the trial value of the θ to make the rescaled curves collapse onto each other, we access the dynamic exponent $\theta = -0.84(4)$.

The negative exponent θ is notably interesting since it is in sharp contrast to classical criticality, in which θ is usually positive. To illustrate the underlying physics, we consider the short-time dynamic behavior from an initial RS state with a small residual magnetization m_0 . By operator product expansion [61], it was shown that the order parameter m evolves as $m \propto m_0 \tau^\theta$ in the short-time stage. This dynamical scaling behavior is the consequence of the competition between the domain expansion of magnetization and the critical fluctuation. In classical cases, the critical fluctuations of order parameter are weak in the short-time stage of evolution, and domain expansion around the seeds of m_0 is dominant, giving rise to a positive θ . This scenario also holds for the quantum Ising model (See the supplementary materials [98]). In contrast, the presence of gapless Dirac fermions strongly enhances the critical fluctuations of magnetization and suppresses the tendency of domain expansion, hence yielding the negative dynamic exponent θ . The negative value of θ offers an extraordinary aspect to witness the fermionic quantum criticality from the perspective of nonequilibrium dynamics.

Discussions and concluding remarks— In summary, we perform sign-problem-free QMC simulation to investigate the imaginary-time relaxation dynamics in a Dirac QCP belonging to chiral Heisenberg universality class. For the first time, we develop scaling forms for different initial states in Dirac QCP and reveal rich nonequilibrium dynamic scaling behaviors. Particularly, a negative critical initial slip exponent $\theta = -0.84(4)$ is observed in the relaxation process from uncorrelated random spin initial state, remarkably different from the classical cases in which θ is positive. The negative critical initial slip exponent unveiled in our study is thus a new manifestation of Dirac QCP, shedding new light on the understanding of QCP in fermionic systems through the lens of short-time dynamic behavior.

Moreover, our study paves a new way to deciphering the critical properties of quantum phase transition in fermionic systems. Based on the dynamic scaling theory, we develop a new framework to determine and verify

critical exponents. Compared with the usual methods tackling critical properties in equilibrium ground state, the nonequilibrium method is highly efficient. In our framework, the critical exponents are accessed by the short imaginary-time evolution, thus significantly reducing the computational time, which is generically proportional to the imaginary time of the evolution in numerical approaches such as QMC. More crucially, our study offers a possible route to studying fermionic QCP in the presence of sign problem, which is the main obstacle hindering the understanding of QCP by numerical approach. Since the severity of sign problem exponentially increases with imaginary time in the process of evolution, the simulation on relatively large system sizes usually remains accessible in the stage of short imaginary time. Hence, it is promising to access the quantum critical behavior even when the model under consideration is sign problematic. Future works along this direction are highly desirable.

Acknowledgments— Y. K. Yu, Z. Zeng and S. Yin are supported by the National Natural Science Foundation of China (Grants No. 12075324 and No. 12222515). Z. X. Li is supported by the start-up grant of IOP-CAS. Y. R. Shu is supported by the National Natural Science Foundation of China (Grant No. 12104109). Y. K. Yu and Z. Zeng are also supported by (national) college students innovation and entrepreneurship training program, Sun Yat-sen University. S. Yin is also supported by the Science and Technology Projects in Guangdong Province (Grants No. 211193863020).

* zixiangli@iphy.ac.cn

† yinsh6@mail.sysu.edu.cn

- [1] S. Sachdev, *Quantum Phase Transitions*, 2nd ed. (Cambridge Univ. Press, 2011).
- [2] D. J. Gross and A. Neveu, *Phys. Rev. D* **10**, 3235 (1974).
- [3] A. H. Castro Neto, F. Guinea, N. M. R. Peres, K. S. Novoselov, and A. K. Geim, *Rev. Mod. Phys.* **81**, 109 (2009).
- [4] M. Z. Hasan and C. L. Kane, *Rev. Mod. Phys.* **82**, 3045 (2010).
- [5] X.-L. Qi and S.-C. Zhang, *Rev. Mod. Phys.* **83**, 1057 (2011).
- [6] L. N. Mihaila, N. Zerf, B. Ihrig, I. F. Herbut, and M. M. Scherer, *Phys. Rev. B* **96**, 165133 (2017).
- [7] N. Zerf, L. N. Mihaila, P. Marquard, I. F. Herbut, and M. M. Scherer, *Phys. Rev. D* **96**, 096010 (2017).
- [8] K. Ladovrechis, S. Ray, T. Meng, and L. Janssen, *Phys. Rev. B* **107**, 035151 (2023).
- [9] L. Janssen and I. F. Herbut, *Phys. Rev. B* **89**, 205403 (2014).
- [10] B. Knorr, *Phys. Rev. B* **94**, 245102 (2016).
- [11] J. A. Gracey, T. Luthe, and Y. Schröder, *Phys. Rev. D* **94**, 125028 (2016).
- [12] B. Roy, V. Juričić, and I. F. Herbut, *Journal of High Energy Physics* **2016**, 18 (2016).
- [13] F. Gehring, H. Gies, and L. Janssen, *Phys. Rev. D* **92**,

- 085046 (2015).
- [14] B. Ihrig, L. N. Mihaila, and M. M. Scherer, *Phys. Rev. B* **98**, 125109 (2018).
 - [15] R. Boyack, H. Yezhakov, and J. Maciejko, *The European Physical Journal Special Topics* **230**, 979 (2021).
 - [16] B. Roy and S. Das Sarma, *Phys. Rev. B* **94**, 115137 (2016).
 - [17] S. Han, G. Y. Cho, and E.-G. Moon, *Phys. Rev. B* **98**, 085149 (2018).
 - [18] D. Poland, S. Rychkov, and A. Vichi, *Rev. Mod. Phys.* **91**, 015002 (2019).
 - [19] T. C. Lang and A. M. Läuchli, *Phys. Rev. Lett.* **123**, 137602 (2019).
 - [20] Z. H. Liu, W. Jiang, B.-B. Chen, J. Rong, M. Cheng, K. Sun, Z. Y. Meng, and F. F. Assaad, *Phys. Rev. Lett.* **130**, 266501 (2023).
 - [21] Z.-X. Li, A. Vaezi, C. B. Mendl, and H. Yao, *Science Advances* **4**, eaau1463 (2018).
 - [22] S. Gazit, M. Randeria, and A. Vishwanath, *Nature Physics* **13**, 484 (2017).
 - [23] Z. Zhou, D. Wang, Z. Y. Meng, Y. Wang, and C. Wu, *Phys. Rev. B* **93**, 245157 (2016).
 - [24] S. M. Tabatabaei, A.-R. Negari, J. Maciejko, and A. Vaezi, *Phys. Rev. Lett.* **128**, 225701 (2022).
 - [25] Y. Otsuka, K. Seki, S. Sorella, and S. Yunoki, *Phys. Rev. B* **98**, 035126 (2018).
 - [26] X. Y. Xu and T. Grover, *Phys. Rev. Lett.* **126**, 217002 (2021).
 - [27] Y. Liu, W. Wang, K. Sun, and Z. Y. Meng, *Phys. Rev. B* **101**, 064308 (2020).
 - [28] S. Chandrasekharan and A. Li, *Phys. Rev. D* **88**, 021701 (2013).
 - [29] X. Zhu, Y. Huang, H. Guo, and S. Feng, *Phys. Rev. B* **106**, 075109 (2022).
 - [30] T.-T. Wang and Z. Y. Meng, “Emus live on the gross-neveu-yukawa archipelago,” (2023), [arXiv:2304.00034](https://arxiv.org/abs/2304.00034) [cond-mat.str-el].
 - [31] X.-J. Yu, Z. Pan, L. Xu, and Z.-X. Li, “Non-hermitian strongly interacting dirac fermions: a quantum monte-carlo study,” (2023), [arXiv:2302.10115](https://arxiv.org/abs/2302.10115) [cond-mat.str-el].
 - [32] H. Xu, X. Li, Z. Zhou, X. Wang, L. Wang, C. Wu, and Y. Wang, *Phys. Rev. Res.* **5**, 023180 (2023).
 - [33] P. Corboz, P. Czarnik, G. Kapteijns, and L. Tagliacozzo, *Phys. Rev. X* **8**, 031031 (2018).
 - [34] M. Rader and A. M. Läuchli, *Phys. Rev. X* **8**, 031030 (2018).
 - [35] S. Sorella and E. Tosatti, *Europhysics Letters* **19**, 699 (1992).
 - [36] I. F. Herbut, *Phys. Rev. Lett.* **97**, 146401 (2006).
 - [37] I. F. Herbut, V. Juričić, and O. Vafeck, *Phys. Rev. B* **80**, 075432 (2009).
 - [38] F. F. Assaad and I. F. Herbut, *Phys. Rev. X* **3**, 031010 (2013).
 - [39] Y. Otsuka, S. Yunoki, and S. Sorella, *Phys. Rev. X* **6**, 011029 (2016).
 - [40] T. Grover, D. N. Sheng, and A. Vishwanath, *Science* **344**, 280 (2014).
 - [41] U. F. P. Seifert, X.-Y. Dong, S. Chuliparambil, M. Vojta, H.-H. Tu, and L. Janssen, *Phys. Rev. Lett.* **125**, 257202 (2020).
 - [42] S. Ray and L. Janssen, *Phys. Rev. B* **104**, 045101 (2021).
 - [43] Y. Da Liao, X. Y. Xu, Z. Y. Meng, and Y. Qi, *Phys. Rev. B* **106**, 075111 (2022).
 - [44] L. Wang, P. Corboz, and M. Troyer, *New Journal of Physics* **16**, 103008 (2014).
 - [45] Z.-X. Li, Y.-F. Jiang, and H. Yao, *New Journal of Physics* **17**, 085003 (2015).
 - [46] Y. Liu, Z. Wang, T. Sato, W. Guo, and F. F. Assaad, *Phys. Rev. B* **104**, 035107 (2021).
 - [47] Z. H. Liu, M. Vojta, F. F. Assaad, and L. Janssen, *Phys. Rev. Lett.* **128**, 087201 (2022).
 - [48] C. Chen, X. Y. Xu, Z. Y. Meng, and M. Hohenadler, *Phys. Rev. Lett.* **122**, 077601 (2019).
 - [49] Y.-X. Zhang, W.-T. Chiu, N. C. Costa, G. G. Batrouni, and R. T. Scalettar, *Phys. Rev. Lett.* **122**, 077602 (2019).
 - [50] Z.-X. Li, Y.-F. Jiang, S.-K. Jian, and H. Yao, *Nature Communications* **8**, 314 (2017).
 - [51] B.-H. Li, Z.-X. Li, and H. Yao, *Phys. Rev. B* **101**, 085105 (2020).
 - [52] E. Torres, L. Classen, I. F. Herbut, and M. M. Scherer, *Phys. Rev. B* **97**, 125137 (2018).
 - [53] L. Classen, I. F. Herbut, and M. M. Scherer, *Phys. Rev. B* **96**, 115132 (2017).
 - [54] Y.-Z. You, Y.-C. He, C. Xu, and A. Vishwanath, *Phys. Rev. X* **8**, 011026 (2018).
 - [55] S. Yin and Z.-Y. Zuo, *Phys. Rev. B* **101**, 155136 (2020).
 - [56] P. C. Hohenberg and B. I. Halperin, *Rev. Mod. Phys.* **49**, 435 (1977).
 - [57] A. Polkovnikov, K. Sengupta, A. Silva, and M. Vengalattore, *Rev. Mod. Phys.* **83**, 863 (2011).
 - [58] J. Dziarmaga, *Advances in Physics* **59**, 1063 (2010).
 - [59] L. D’Alessio, Y. Kafri, A. Polkovnikov, and M. Rigol, *Advances in Physics* **65**, 239 (2016).
 - [60] A. Mitra, *Annual Review of Condensed Matter Physics* **9**, 245 (2018).
 - [61] H. K. Janssen, B. Schaub, and B. Schmittmann, *Zeitschrift für Physik B Condensed Matter* **73**, 539 (2014).
 - [62] Z. B. Li, L. Schülke, and B. Zheng, *Phys. Rev. Lett.* **74**, 3396 (1995).
 - [63] E. V. Albano, M. A. Bab, G. Baglietto, R. A. Borzi, T. S. Grigera, E. S. Lascar, D. E. Rodriguez, M. L. R. Puzzo, and G. P. Saracco, *Reports on Progress in Physics* **74**, 026501 (2011).
 - [64] E. G. Dalla Torre, E. Demler, and A. Polkovnikov, *Phys. Rev. Lett.* **110**, 090404 (2013).
 - [65] P. Gagel, P. P. Orth, and J. Schmalian, *Phys. Rev. Lett.* **113**, 220401 (2014).
 - [66] P. Gagel, P. P. Orth, and J. Schmalian, *Phys. Rev. B* **92**, 115121 (2015).
 - [67] A. Chiocchetta, M. Tavora, A. Gambassi, and A. Mitra, *Phys. Rev. B* **91**, 220302 (2015).
 - [68] A. Chiocchetta, A. Gambassi, S. Diehl, and J. Marino, *Phys. Rev. Lett.* **118**, 135701 (2017).
 - [69] S.-K. Jian, S. Yin, and B. Swingle, *Phys. Rev. Lett.* **123**, 170606 (2019).
 - [70] S. Yin and S.-K. Jian, *Phys. Rev. B* **103**, 125116 (2021).
 - [71] J. Marino, M. Eckstein, M. S. Foster, and A. M. Rey, *Reports on Progress in Physics* **85**, 116001 (2022).
 - [72] W. Hou and Y.-Z. You, *Phys. Rev. B* **108**, 125130 (2023).
 - [73] M. Motta, C. Sun, A. T. K. Tan, M. J. O’Rourke, E. Ye, A. J. Minnich, F. G. S. L. Brandão, and G. K.-L. Chan, *Nature Physics* **16**, 205 (2020).
 - [74] H. Nishi, T. Kosugi, and Y.-i. Matsushita, *npj Quantum Information* **7**, 85 (2021).
 - [75] S.-H. Lin, R. Dilip, A. G. Green, A. Smith, and F. Pollmann, *PRX Quantum* **2**, 010342 (2021).
 - [76] K. J. Satzinger, Y.-J. Liu, A. Smith, C. Knapp,

- M. Newman, C. Jones, Z. Chen, C. Quintana, X. Mi, A. Dunsworth, C. Gidney, I. Aleiner, F. Arute, K. Arya, J. Atalaya, R. Babbush, J. C. Bardin, R. Barends, J. Basso, A. Bengtsson, A. Bilmes, M. Broughton, B. B. Buckley, D. A. Buell, B. Burkett, N. Bushnell, B. Chiaro, R. Collins, W. Courtney, S. Demura, A. R. Derk, D. Eppens, C. Erickson, L. Faoro, E. Farhi, A. G. Fowler, B. Foxen, M. Giustina, A. Greene, J. A. Gross, M. P. Harrigan, S. D. Harrington, J. Hilton, S. Hong, T. Huang, W. J. Huggins, L. B. Ioffe, S. V. Isakov, E. Jeffrey, Z. Jiang, D. Kafri, K. Kechedzhi, T. Khattar, S. Kim, P. V. Klimov, A. N. Korotkov, F. Kostritsa, D. Landhuis, P. Laptev, A. Locharla, E. Lucero, O. Martin, J. R. McClean, M. McEwen, K. C. Miao, M. Mohseni, S. Montazeri, W. Mruczkiewicz, J. Mutus, O. Naaman, M. Neeley, C. Neill, M. Y. Niu, T. E. Orien, A. Opremcak, B. Pat, A. Petukhov, N. C. Rubin, D. Sank, V. Shvarts, D. Strain, M. Szalay, B. Villalonga, T. C. White, Z. Yao, P. Yeh, J. Yoo, A. Zalcman, H. Neven, S. Boixo, A. Megrant, Y. Chen, J. Kelly, V. Smelyanskiy, A. Kitaev, M. Knap, F. Pollmann, and P. Roushan, *Science* **374**, 1237 (2021).
- [77] G. Semeghini, H. Levine, A. Keesling, S. Ebadi, T. T. Wang, D. Bluvstein, R. Verresen, H. Pichler, M. Kalinowski, R. Samajdar, A. Omran, S. Sachdev, A. Vishwanath, M. Greiner, V. Vuleti, and M. D. Lukin, *Science* **374**, 1242 (2021).
- [78] C. De Grandi, A. Polkovnikov, and A. W. Sandvik, *Phys. Rev. B* **84**, 224303 (2011).
- [79] C. De Grandi, A. Polkovnikov, and A. W. Sandvik, *Journal of Physics: Condensed Matter* **25**, 404216 (2013).
- [80] C.-W. Liu, A. Polkovnikov, and A. W. Sandvik, *Phys. Rev. B* **87**, 174302 (2013).
- [81] S. Yin, P. Mai, and F. Zhong, *Phys. Rev. B* **89**, 144115 (2014).
- [82] S. Zhang, S. Yin, and F. Zhong, *Phys. Rev. E* **90**, 042104 (2014).
- [83] Y.-R. Shu, S.-K. Jian, and S. Yin, *Phys. Rev. Lett.* **128**, 020601 (2022).
- [84] Y.-R. Shu and S. Yin, *Phys. Rev. B* **105**, 104420 (2022).
- [85] Z. Zuo, S. Yin, X. Cao, and F. Zhong, *Phys. Rev. B* **104**, 214108 (2021).
- [86] S.-X. Zhang and S. Yin, “Universal imaginary-time critical dynamics on a quantum computer,” (2023), [arXiv:2308.05408 \[quant-ph\]](https://arxiv.org/abs/2308.05408).
- [87] S. Sorella, S. Baroni, R. Car, and M. Parrinello, *Europhysics Letters* **8**, 663 (1989).
- [88] F. Assaad and H. Evertz, “World-line and determinantal quantum monte carlo methods for spins, phonons and electrons,” in *Computational Many-Particle Physics*, edited by H. Fehske, R. Schneider, and A. Weiße (Springer Berlin Heidelberg, Berlin, Heidelberg, 2008) pp. 277–356.
- [89] Z.-X. Li and H. Yao, *Annual Review of Condensed Matter Physics* **10**, 337 (2019), <https://doi.org/10.1146/annurev-conmatphys-033117-054307>.
- [90] M. Troyer and U.-J. Wiese, *Phys. Rev. Lett.* **94**, 170201 (2005).
- [91] C. Wu and S.-C. Zhang, *Phys. Rev. B* **71**, 155115 (2005).
- [92] Z.-X. Li, Y.-F. Jiang, and H. Yao, *Phys. Rev. B* **91**, 241117 (2015).
- [93] Z.-X. Li, Y.-F. Jiang, and H. Yao, *Phys. Rev. Lett.* **117**, 267002 (2016).
- [94] Z. C. Wei, C. Wu, Y. Li, S. Zhang, and T. Xiang, *Phys. Rev. Lett.* **116**, 250601 (2016).
- [95] E. Berg, M. A. Metlitski, and S. Sachdev, *Science* **338**, 1606 (2012).
- [96] B. Zheng, *Phys. Rev. Lett.* **77**, 679 (1996).
- [97] F. Parisen Toldin, M. Hohenadler, F. F. Assaad, and I. F. Herbut, *Phys. Rev. B* **91**, 165108 (2015).
- [98] See the supplementary materials for more information.
- [99] Y.-R. Shu, S. Yin, and D.-X. Yao, *Phys. Rev. B* **96**, 094304 (2017).

Supplementary Materials for

Nonequilibrium dynamics in Dirac quantum criticality

DETERMINANT QUANTUM MONTE CARLO

We employ the large-scale determinant quantum Monte Carlo (DQMC) method [88] to investigate the imaginary-time relaxation dynamics of our model. Specifically, we prepare an initial state $|\psi_0\rangle$ and set the system parameters U/t on the critical point to observe the scaling behavior of observables during the short-time stage. When the system evolves to imaginary time τ , the expectation value of observables is given by

$$\langle O(\tau) \rangle = \frac{\langle \psi_0 | e^{-\frac{\tau}{2}H} O e^{-\frac{\tau}{2}H} | \psi_0 \rangle}{\langle \psi_0 | e^{-\tau H} | \psi_0 \rangle}. \quad (S1)$$

Herein, the imaginary-time propagator acts on the initial state, projecting it closer to the ground state. Hence, the DQMC framework under this context is also termed propagator quantum Monte Carlo (PQMC). In numerical calculations, we use Trotter decomposition to discretize imaginary-time propagator into $M = \tau/\Delta\tau$ (M is integer) time slices with

$$e^{-\tau H} = \prod_{m=1}^M [e^{-\Delta\tau H_t} e^{-\Delta\tau H_U} + \mathcal{O}(\Delta\tau^2)], \quad (S2)$$

where H_t and H_U are the hopping term and Hubbard interaction term respectively in the Hamiltonian. We choose small enough $\Delta\tau/t < 0.05$. To decouple two-body fermion-fermion coupling form of $e^{\Delta\tau H_U}$, we use a discrete Hubbard-Stratonovich transformation

$$e^{-\frac{\Delta\tau U}{2}(n_{i\uparrow}+n_{i\downarrow}-1)^2} = \sum_{l=\pm 1, \pm 2} \gamma(l) e^{i\sqrt{\frac{\Delta\tau U}{2}}\eta(l)(n_{i\uparrow}+n_{i\downarrow}-1)}, \quad (S3)$$

to obtain one-body fermion-auxiliary field coupling. Here, we introduce a four-component space-time local auxiliary fields $\gamma(\pm 1) = 1 + \sqrt{6}/3$, $\gamma(\pm 2) = 1 - \sqrt{6}/3$, $\eta(\pm 1) = \pm\sqrt{2(3-\sqrt{6})}$, $\eta(\pm 2) = \pm\sqrt{2(3+\sqrt{6})}$, and use DQMC for importance sampling over these space-time configurations. Next, we elaborate on how DQMC numerically calculates the sampling weight.

For each imaginary time and each position of the Hubbard interaction, we employ an Hubbard-Stratonovich transformation as in Eq. (S3). This means that we introduce an auxiliary field in $d+1$ dimensions. As a result, the imaginary-time propagator can be fully expressed using single-particle operators. This allows us to represent it in the following quadratic form of fermion operators:

$$e^{-\tau H} \equiv \sum_{\mathbf{c}} e^{-\tau H_{\mathbf{c}}} = \sum_{\mathbf{c}} A_{\mathbf{c}} \prod_{m=1}^M e^{\vec{c}^\dagger T \vec{c}} e^{\vec{c}^\dagger V_{\mathbf{c}(m)} \vec{c}}, \quad (S4)$$

where $\sum_{\mathbf{c}}$ denotes the summation over all space-time configurations of the auxiliary field. Considering that each local component of the auxiliary field has 4 possible values, the summation comprises up to 4^{MN} terms, where N represents the number of spatial degrees of freedom. $H_{\mathbf{c}}$ denotes the decoupled configuration Hamiltonian, while T and $V_{\mathbf{c}(m)}$ are the resulting quadratic coefficient matrices from the rearrangement, and $A_{\mathbf{c}}$ is the coefficient. Both $V_{\mathbf{c}(m)}$ and $A_{\mathbf{c}}$ depend on the auxiliary field configuration. The complete form of the evolution operator has been presented above. Next, we consider expressing the initial state. The AFM, DSM, RS initial states we use are all direct product states, and numerically they can be written as the following Slater determinant:

$$|\psi_0\rangle = \bigotimes_{n_e=1}^{N_e} \left[\left(\sum_x c_x^\dagger P_{x,n_e} \right) |0\rangle \right] = \bigotimes_{n_e=1}^{N_e} \left[(\vec{c}^\dagger P)_{n_e} |0\rangle \right], \quad (S5)$$

where N_e denotes the number of electrons. This implies that the initial state is a direct product of N_e fermion single-particle wave functions. The index x denotes the degree of freedom of the electron, including spatial degrees of freedom, spin degrees of freedom, etc. The matrix element P_{x,n_e} represents the probability amplitude of the n_e th

electron on the x th degree of freedom. Note that the imaginary-time propagator $e^{-\tau H_c}$ is essentially the Boltzmann weight factor of the auxiliary field configuration in statistical mechanics. According to Eqs. (S4) and (S5), the partition function of the auxiliary field configuration can be expressed as:

$$Z = \sum_c \langle \psi_0 | e^{-\tau H_c} | \psi_0 \rangle = \sum_c A_c \det [P^\dagger B_c(\tau, 0) P]. \quad (\text{S6})$$

Here, we use B_c to represent the exponential of the quadratic coefficient matrix:

$$B_c(\tau_2, \tau_1) \equiv \prod_{m=\tau_1/\Delta\tau}^{\tau_2/\Delta\tau} e^T e^{V_{c(m)}}. \quad (\text{S7})$$

The expression on the right side of Eq. (S6) has integrated out the fermion operators, replacing the Grassmann numbers and fermion statistics, with a determinant representation that is computationally tractable. All matrix operations can be performed directly on a computer.

Ultimately, our Monte Carlo sampling is conducted over space-time configurations. Numerically, the weight of a space-time configuration is $A_c \det [P^\dagger B_c(\tau, 0) P]$. Following the classical Markov importance sampling method, we continuously make tentative flips to the local components of this $d + 1$ dimensional auxiliary field. We then employ the Metropolis algorithm to calculate the probability of accepting these changes based on the ratio of configuration weights before and after the flip. Specifically, we need to compute the following weight ratio:

$$R_{c'c} \equiv \frac{A_{c'} \det [P^\dagger B_{c'}(\tau, 0) P]}{A_c \det [P^\dagger B_c(\tau, 0) P]}, \quad (\text{S8})$$

where c' represents the flipped configuration and c represents the original configuration. In fact, we do not need to compute the weights of the two configurations separately. This is because the flipping we perform is localized in space-time, so

$$B_{c'}(\tau, 0) = B_c(\tau, \zeta) (\mathbb{1} + \Delta_{c'c}) B_c(\zeta, 0). \quad (\text{S9})$$

Here, $\Delta_{c'c}$ is a highly sparse matrix, where only the matrix elements corresponding to the degrees of freedom involved in the local auxiliary field flipping are non-zero. Thus, the ratio of the two determinants can be expressed as:

$$\frac{\det [P^\dagger B_{c'}(\tau, 0) P]}{\det [P^\dagger B_c(\tau, 0) P]} = \det \left\{ \mathbb{1} + \Delta_{c'c} B_c(\zeta, 0) P [P^\dagger B_c(\tau, 0) P]^{-1} P^\dagger B_c(\tau, \zeta) \right\}. \quad (\text{S10})$$

Due to the sparsity of $\Delta_{c'c}$, the determinant on the right side of the above equation only requires consideration of a few degrees of freedom involved in the flipping during computations.

In DQMC, to compute the physical observables, we only need to statistically analyze the configurational observable $\langle O(\tau) \rangle_c$.

$$\langle O(\tau) \rangle = \sum_c \text{Pr}_c \langle O(\tau) \rangle_c + \mathcal{O}(\Delta\tau^2), \quad (\text{S11})$$

where Pr_c represents the configuration probability,

$$\text{Pr}_c = \frac{1}{Z} A_c \det [P^\dagger B_c(\tau, 0) P], \quad (\text{S12})$$

$$\langle O(\tau) \rangle_c = \frac{\langle \psi_0 | e^{-\frac{\tau}{2} H_c} O e^{-\frac{\tau}{2} H_c} | \psi_0 \rangle}{\langle \psi_0 | e^{-\tau H_c} | \psi_0 \rangle}. \quad (\text{S13})$$

Since we employ importance sampling, the sampling frequency is proportional to the configuration probability. Ultimately, when calculating the observable, we simply take the average over the sampled configurational observables. If the observable is a single-particle operator, meaning it can be expressed as a quadratic form of fermion operators, then one can integrate out the fermion degrees of freedom in a manner similar to Eq. (S6) and numerically compute using determinants. For observables of four-fermion operators or higher, we compute using the fermion equal-time Green's function based on Wick's theorem. After numerically integrating out the fermion degrees of freedom, the fermion equal-time Green's function can be expressed using the following matrix element:

$$\langle c_{x_1}^\dagger c_{x_2} \rangle_c = \left\{ B_c \left(\frac{\tau}{2}, 0 \right) P [P^\dagger B_c(\tau, 0) P]^{-1} P^\dagger B_c \left(\tau, \frac{\tau}{2} \right) \right\}_{x_1, x_2}. \quad (\text{S14})$$

DETERMINATION OF THE CRITICAL POINT

Here we offer supplementary details and numerical insights on pinpointing the critical point. In Fig. 2(a) of the paper, we show that different sizes of R - U curves intersect at the critical point when τL^{-z} is taken as 0.3, 0.34, and 0.5. However, due to finite size effects, there may be slight deviations between the intersection points of small-sized curves and the real critical point. We denote the intersection points of size L and $L+3$ as $U_c(L)$, which are shown in Fig. S1. The accuracy of these intersection points is highly susceptible to errors from data points near the intersections, especially given the small angles at which the curves cross.

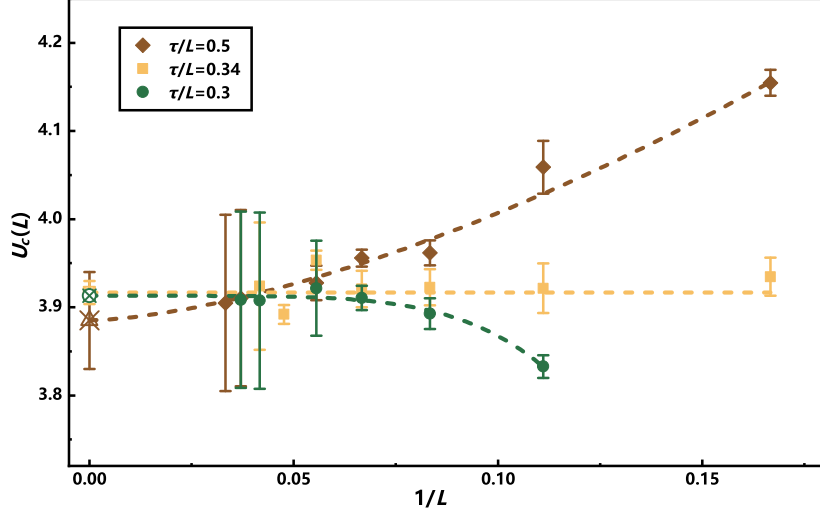


FIG. S1. Determine the critical point by extrapolation. When τL^{-z} is fixed at 0.3, 0.34, and 0.5 respectively, the intersection points $U_c(L)$ of the R - U curves for sizes L and $L+3$ are shown in the figure. The critical point is extrapolated when the system tends to thermodynamic limit $L \rightarrow \infty$. Note that the extrapolation results are also marked at $1/L = 0$.

We extrapolate the critical point outside the thermodynamic limit $L \rightarrow \infty$ using the form $U_c(L) = U_c + aL^{-w}$. The intercept shown in Fig. S1 represents the extrapolated critical point. For three different cases of $\tau L^{-z} = 0.3, 0.34, 0.5$, our results are $U_c = 3.91(3), 3.92(1), 3.88(4)$ respectively. They all extrapolate to the same limit within the error range, thus demonstrating that our method based on nonequilibrium information to determine critical points using dynamic scaling is reliable.

The relaxation-dynamics-based method we used above to solve the critical point can be applied universally to other fermion systems. Nevertheless, it is worth mentioning that as shown in Fig. S1, the $U_c(L)$ approaches the critical point with different trends as L increases when different values of τ/L are taken. Specifically, when $\tau/L = 0.3$, the $U_c(L)$ under small size is smaller than the real critical point at thermodynamic limit; while when $\tau/L = 0.5$, the $U_c(L)$ under small size is larger than the real critical point; even more interestingly, we found that at $\tau/L = 0.34$, the $U_c(L)$ almost does not depend on size and can exhibit a real critical behavior under small sizes alone. This means that in the short-time stage, the $U_c(L)$ of the system tends to lean towards disordered phase, while after a long-time evolution, it leans towards ordered phase. This reversal of $U_c(L)$ shift has not been observed in previous phase transitions of bosonic systems and spin systems. We are not sure if this phenomenon is universal, and more research on the nonequilibrium of fermionic systems is needed.

MORE RESULTS ABOUT THE CRITICAL EXPONENTS

In the main text, we use the data with fixed $\tau L^{-z} = 0.3$ to determine the critical exponent ν . Here, we supplement the results of $\tau L^{-z} = 0.5$ and 0.34. Fig. S2 shows the curves of different sizes' correlation-length ratios changing with U/t . We adjust the rescaling parameters U_c and ν to make the curves of different sizes coincide. To avoid finite size effects as much as possible, we fit U_c and ν using curves above $L = 12$. For $\tau L^{-z} = 0.5$ and 0.34, we obtain results of $U_c = 3.91(2)$ and $3.92(4)$, respectively, as well as $\nu = 1.22(6)$ and $1.22(17)$. They are consistent with our results presented in the paper within error range.

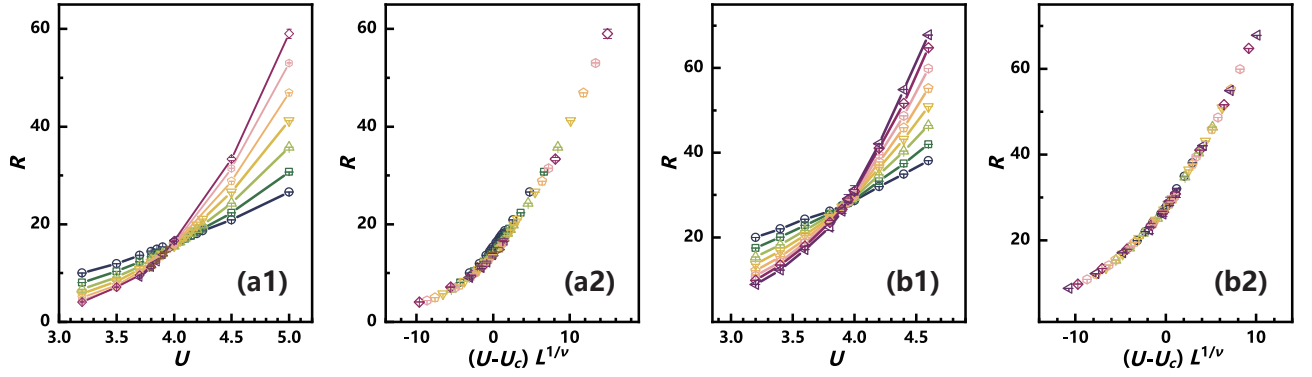


FIG. S2. The variation of the correlation-length ratio with respect to U/t at fixed τL^{-z} . (a1) display the results obtained by setting $\tau L^{-z} = 0.5$. (a2) shows rescaling is applied to the horizontal axis of (a1). (b1) display the results obtained by setting $\tau L^{-z} = 0.34$. (b2) shows rescaling is applied to the horizontal axis of (b1).

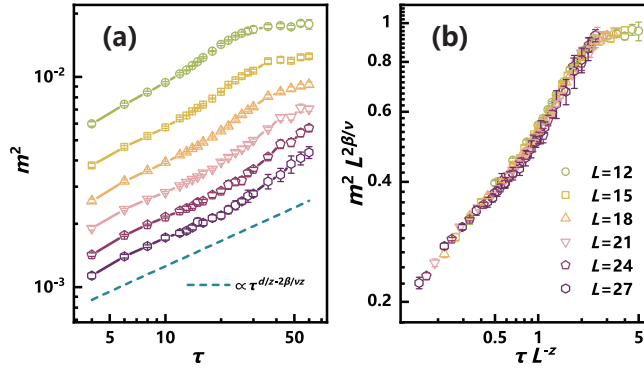


FIG. S3. Relaxation behavior of order parameter with the RS initial state. (a) shows that the order parameter for large size L increases in a form close to $\tau^{d/z-2\beta/\nu z}$. (b) has been rescaled on both axes, and curves of different sizes L overlap. The critical exponent value chosen here is $\beta/\nu = 0.80$.

Furthermore, by using these results for rescaling, in Fig. S2 (a2), it can be seen that for $\tau L^{-z} = 0.5$, small-size curves do not completely coincide with large-size curves; while in Fig. S2 (b2), it is shown that even small-size curves can coincide very well for $\tau L^{-z} = 0.34$, which also confirms what we mentioned in the previous section.

In the main text, we also examine the scaling form and critical exponents in relaxation dynamics with Dirac semi-metal (DSM) initial state. Here, we base our examination on relaxation dynamics with random spin (RS) initial state. We show in Fig. S3 the variation of the square of the order parameter during the relaxation with RS initial state. The relaxation scaling used to describe DSM initial states in our paper is also applicable here, but with different specific scaling function. At the critical point, it takes a slightly longer time for RS initial states to relax to equilibrium compared to DSM initial states because the latter are actually correlated while the former are completely random.

In short-time stage, τL^{-z} is small enough that scaling function $f_{m^2}(\tau L^{-z})$ can be approximated as a constant. Therefore, for a given size $m^2 \propto \tau^{d/z-2\beta/\nu z}$ and different sizes L , their relaxation curves do not overlap in short-time stage due to the factor of L^{-d} in proportionality coefficient, but they follow the same power law with increasing τ . As shown in Fig. S3 (a), different curves are approximately parallel with slope $d/z - 2\beta/\nu z$. In Fig. S3 (b), we also verify the critical exponent $\beta/\nu = 0.80$ obtained from the relaxation dynamics of AFM initial state. We rescale the relaxation dynamics of DSM initial state using this result and find that curves of different sizes L overlap, which self-consistently confirms our results.

CRITICAL INITIAL SLIP IN QUANTUM ISING MODELS

In the main text, we determine the critical initial slip exponent θ of the Dirac fermions through the critical relaxation behavior of the auto-correlation function A . Here, we study the critical dynamics of the auto-correlation function A

in the 1D and 2D transverse-field Ising models. In previous works [81, 99], the critical initial slip exponent for the 1D and 2D Ising models is obtained from other methods. Here, we show that the critical initial slip exponent for these models can also be obtained from the scaling of A . Figure S4 (a1) shows the relaxation process of A for various sizes of the 1D transverse-field Ising model at the critical point $h/J = 1$. In Fig. S4 (a2), we rescale the relaxation process for 1D. Here, we take $\theta = 0.3734$ [99] and $z = 1$. After rescaling, the relaxation curves of different sizes overlap, satisfying the scaling relation for A as mentioned in our main text. For the 2D transverse-field Ising model at the critical point $h/J = 3.04451$, we performed similar numerical simulations, as shown in Fig. S4 (b1). The relaxation curves of various sizes of A overlap when rescaled with $\theta = 0.209$ [99], as shown in Fig. S4 (b2). Note that for both 1D and 2D quantum Ising models, the critical initial slip exponent is positive.

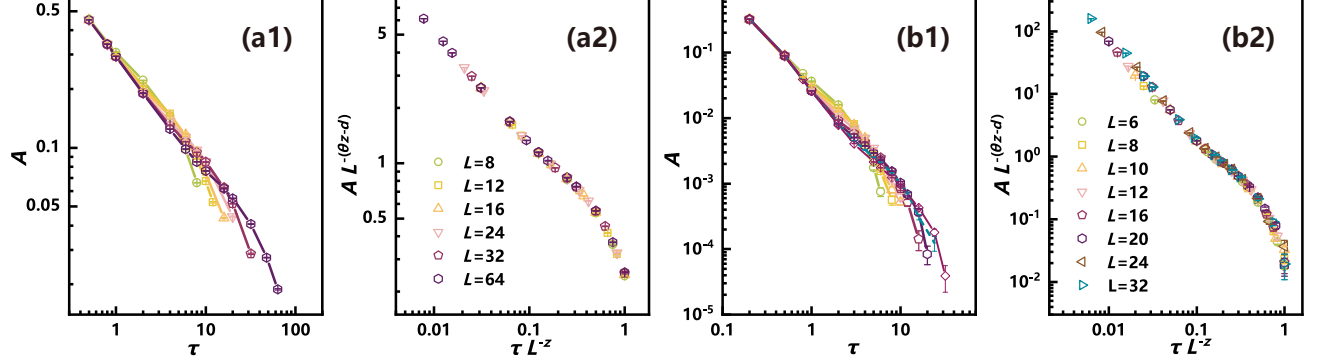


FIG. S4. The relaxation behavior of the auto-correlation function A in the quantum Ising model. (a1) and (b1) respectively show the results in 1D and 2D. (a2) and (b2) are their rescaled results, where the relaxation curves of different sizes overlap.